NANO LETTERS

Letter

pubs.acs.org/NanoLett

Few-Electron Edge-State Quantum Dots in a Silicon Nanowire Field-Effect Transistor

Benoit Voisin,[†] Viet-Hung Nguyen,[‡] Julien Renard,[†] Xavier Jehl,[†] Sylvain Barraud,[§] François Triozon,[§] Maud Vinet,[§] Ivan Duchemin,[‡] Yann-Michel Niquet,[‡] Silvano de Franceschi,[†] and Marc Sanquer*[,†]

[†]SPSMS, UMR-E CEA/UJF-Grenoble 1, INAC, 17 rue des Martyrs, 38054 Grenoble, France

[‡]SPMM, UMR-E CEA/UJF-Grenoble 1, INAC, 17 rue des Martyrs, 38054 Grenoble, France

[§]CEA, LETI, MINATEC Campus, 17 rue des Martyrs, 38054 Grenoble, France

Supporting Information

ABSTRACT: We investigate the gate-induced onset of few-electron regime through the undoped channel of a silicon nanowire field-effect transistor. By combining low-temperature transport measurements and self-consistent calculations, we reveal the formation of one-dimensional conduction modes localized at the two upper edges of the channel. Charge traps in the gate dielectric cause electron localization along these edge modes, creating elongated quantum dots with characteristic lengths of ∼10 nm. We observe single-electron tunneling across two such dots in parallel, specifically one in each channel edge. We identify the filling of these quantum dots with the first few electrons, measuring addition energies of a few tens of millielectron volts and level spacings of the order of 1 meV, which we ascribe to the valley orbit splitting. The total removal of valley degeneracy leaves only a 2-fold spin degeneracy, making edge quantum dots potentially promising candidates for silicon spin qubits.

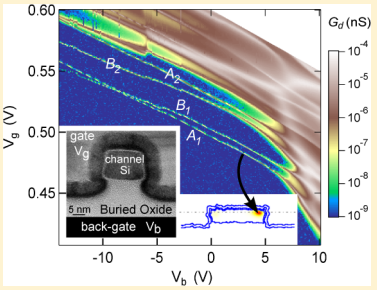

KEYWORDS: *Silicon nanowire, silicon single electron transistor, edge state, quantum dot, valley splitting*

The rapid progress toward ever shorter transistor channels has fostered the development of nanowire field-effect transistors (NW-FETs) based on silicon-on-insulator (SOI) technology. In these transistors, source and drain contacts are connected by a silicon nanowire channel with rectangular cross-section defined through vertical dry etching of the SOI surface layer. The case where the gate electrode covers uniformly three of the four facets of the silicon nanowire (i.e., all except the bottom one) is commonly referred to as the trigate geometry. This configuration provides an excellent compromise between gate efficiency and processability, the most efficient gate-all-around option being technologically very challenging.[1]

A trigate NW-FET turns on by increasing the gate voltage above the so-called threshold voltage. The way channel conduction gets activated is nontrivial though. It has been argued that, due to focusing of the gate field lines, channel formation occurs initially at the two upper edges of the silicon channel, resulting in the formation of localized one-dimensional conduction modes parallel to the channel axis.[2−4] Here we report a low-temperature transport experiment where we identify the gate-induced addition of the first few electrons to the edge modes. We find that the first added electrons are strongly localized due to the disorder potential arising mainly from charged traps in the gate dielectric, an interpretation supported by numerical simulations. This localization leads to quantum-dot behavior and to the emergence of Coulomb blockade effect at low temperature. We clearly observe the few-electron filling of two quantum dots, one for each edge mode. The quantum dots exhibit charging energies of a few tens of millielectron volts and a complete lifting of the valley degeneracy. By performing single-electron tunneling spectroscopy in a magnetic field, we probe the spin character of the quantum dot states. For even occupancy, the ground state is a spin singlet, denoting a filling of the quantum dot levels by pairs of electrons with opposite spin. For odd occupancy, we observe a spin-1/2 ground state whose 2-fold spin degeneracy is lifted by an applied magnetic field. Therefore, the formation of edge quantum dots, demonstrated here for a trigate NW-FET, points to a promising opportunity for the realization of spin-based qubits in intrinsic silicon.

Our trigate NW-FETs were fabricated in a complementary metal−oxide semiconductor (CMOS) platform starting from 300 mm undoped SOI wafers. A 200-nm-long, 11-nm-thick, and 40-nm-wide silicon nanowire was etched out of the undoped SOI. A device schematic is shown in Figure 1a. The central portion of the silicon nanowire was covered by a 54-nm-wide trigate electrode consisting of SiO_2(0.8 nm)/HfSiON(1.9 nm) for the oxide followed by TiN(5 nm)/poly-Si(50 nm). A voltage called V_g is applied on this gate. The silicon regions not covered by the trigate, and its spacers were overgrown and implanted with As donors in order to form n-type, low-resistive source (S) and drain (D) leads. Transport measurements were

Received: January 24, 2014
Revised: March 5, 2014
Published: March 10, 2014

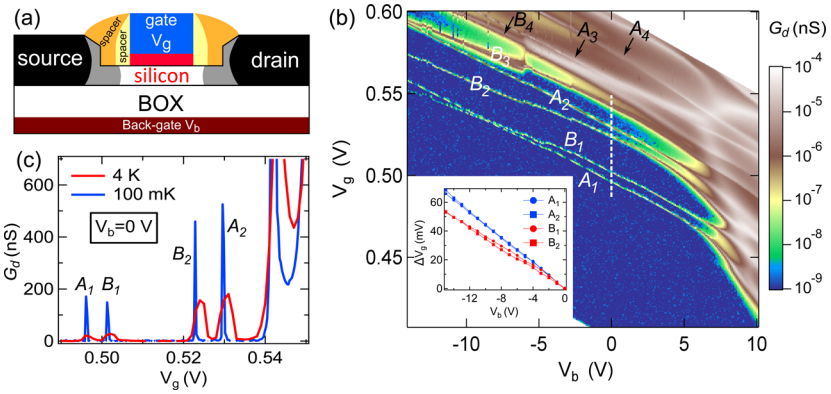

Figure 1. (a) Layout of the studied sample featuring the thin intrinsic silicon channel below the gate stack and the use of two spacers to optimize the source−drain contacts (schematic, not to scale). A transmission electron microscope (TEM) view is presented in the Supporting Information. (b) Source−drain Conductance G_d versus V_b, V_g at T = 0.1 K. Five isolated resonances are identified corresponding to the addition of one electron in the dots. A_1 and A_2 are attributed to the addition of two electrons in the first edge state, and B_1, B_2, and B_3 are attributed to the addition of three electrons in the second edge state. Other higher energy lines are indicated by arrows above the onset. The edge states disappear by hybridization with the bulk conduction channel at positive V_b. Dot A shows a larger charging energy than dot B. The inset shows the shift of the resonance versus V_b and V_g for A_1, A_2, B_1, and B_2. Different charge states of the same edge show the same coupling ratio C_b/C_g, while the states located on different edges have slightly different couplings ($C_b/C_g = 4.5 \times 10^{-3}$ for A and 3.6×10^{-3} for B). (c) A cut of panel (b) along the white dotted line (V_b = 0 V) at T = 0.1 K and T = 4.2 K.

carried out in a dilution refrigerator at a base electron temperature of 100 mK. Importantly, the undoped silicon substrate was used as photoactivated back gate electrode (called V_b) following a method introduced in ref 5. The S−D differential conductance G_d was measured by standard lock-in detection, superimposing an AC modulation of 10−100 μV to a DC S−D bias voltage. Additional details on device fabrication and measurement setup can be found in the Supporting Information.

Figure 1b shows a color plot of G_d versus (V_b, V_g). For our specific gate stack, the threshold voltage is expected to have a value around V_g = +0.5 V when no voltage is applied to the back gate.[6] Indeed, a line cut at V_b = 0 V (see Figure 1c) shows a few conductance resonances just around V_g = +0.5 V and a steep increase of G_d above V_g = +0.55 V. While the latter corresponds to the onset of bulk diffusive transport throughout the channel, the sharp resonances denote resonant tunneling conduction through discrete quantum states.

These discrete states cannot be attributed to shallow donors in the body of the channel,[7,8] as no intentional channel doping has been introduced and as the spacers and the relatively large gate length prevent donors from diffusing from the source and drain regions deep into the channel. Consequently, we are left with the possibility that the observed resonances are due to discrete states resulting from the electrostatic confinement of conduction-band electrons.

To investigate this possibility, we have performed a realistic simulation of the device using a self-consistent nonequilibrium Green's functions (NEGF) code[9] in the effective-mass approximation. Figure 2 shows the carrier distribution when there is one electron in the channel at a negative back-gate bias V_b = −8 V. The simulation only includes the first 11-nm-thick spacer separating the gated channel from the doped source and drain (dopant concentration $N_d = 5 \times 10^{19}$ cm^{-3} with a typical decay length of 5 nm/decade under the spacer). We have checked that overgrown source and drain contacts (as in Figure 1a) have little influence on the potential landscape near the channel and we have not, therefore, systematically included them in the simulation for numerical efficiency. The calculation was carried out at 77 K in order to facilitate numerical

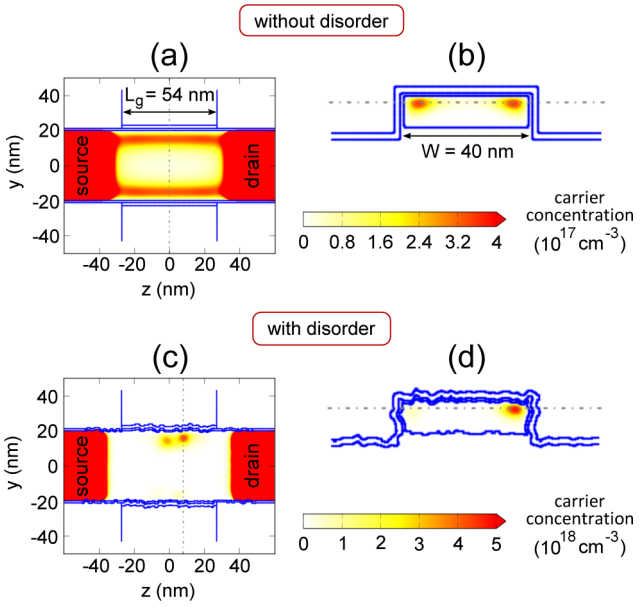

Figure 2. Simulation of the carrier concentration in our devices at T = 77 K and V_b = −8 V. The integrated carrier concentration over the channel (defined as $z \in [-25, 25]$ nm) equals one electron for every figure. The top panel (a and b) corresponds to the nondisordered case: accumulation starts in two symmetric extended edge channels. In the bottom panel (c and d), surface roughness and remote positive charges were introduced in the gate stack. While the carriers are still confined along the top edges of the channel, the mesoscopic variability breaks the left/right symmetry. Near the threshold voltage, the positive charges in the gate dielectric produce a confinement potential for the electrons in the edge states responsible for the quantum dots seen in the experiment.

convergence. We show different cross-sectional views of the device, either parallel (Figure 2a and c) or perpendicular to the channel (Figure 2b and d). In Figure 2a and b, we assume no static disorder: accumulation occurs symmetrically at the top longitudinal edges of the nanowire. With such thin spacers, there is little confinement along the nanowire axis, so that the

dx.doi.org/10.1021/nl500299h | Nano Lett. 2014, 14, 2094−2098

carriers accumulate in one-dimensional conduction modes (see Supporting Information for the simulation of larger spacers). Yet such delocalized modes cannot account for the observed conductance resonances. In Figure 2c and d, we have introduced surface roughness (SR) and positive remote Coulomb (RC) charges[10] at the SiO_2/HfSiON interface. The parameters of the SR profile (Gaussian autocorrelation function[11] with rms Δ = 0.4 nm and correlation length L_c = 1.3 nm) and the density of RC traps ($n_{RC} = 1.5 \times 10^{13}$ cm^{-2}) were chosen to reproduce the experimental mobility of the device at T = 300 K (about 300 cm^2 V^{-1} s^{-1} at a surface carrier concentration of $n_s = 2 \times 10^{12}$ cm^{-2}). The resulting disorder potential breaks the one-dimensional character of the edge states and the symmetry between the left/right edges (see Supporting Information). Near the threshold voltage, localization is mainly driven by the RC charges below the gate. The attractive potential induced by the positive RC charges indeed leads to the formation of small quantum dots located around the center of the channel edges and extending over ~10 nm. In the particular case shown in Figure 2c and d, the first electron is added to a quantum dot formed on the right edge.

We ascribe the conductance resonances observed in Figure 1 to two quantum dots located at the left and right top edges, respectively. This association rests essentially on the following arguments. To a first approximation, tunneling resonances due to the addition of electrons to the same quantum dot produce parallel conductance ridges in the (V_b, V_g) plane (here the importance of using the back gate as an additional control knob). In Figure 1b we can identify two clearly distinct slopes implying the existence of two quantum dots, which we call dot A and dot B. G_d resonances labeled as A_1, ..., A_4 correspond to the addition of the first four electrons to dot A. Their slope gives a ratio $C_b/C_g = 4.5 \times 10^{-3}$, where C_b and C_g are the coupling capacitances between quantum dot A and the bottom and top gate, respectively. G_d resonances labeled as B_1, ..., B_4 are associated with the addition of the first four electrons to dot B. In this case $C_b/C_g = 3.6 \times 10^{-3}$. Note that resonances A_3, A_4, B_3, and B_4 are within the bulk conduction regime suggesting a strong hybridization of the corresponding quantum-dot states with the bulk conduction states and with the source and drain contacts.

Small C_b/C_g values are consistent with a location of the quantum dots in the upper edges of the channel, where the effect of the bottom gate is strongly screened by the metal trigate. Yet this does not tell whether dots A and B are or not on the same edge mode. Quantum dots in parallel yield very different transport signatures from quantum dots in series. In the latter case transport requires a precise alignment of the quantum dot levels, which is not compatible with the resonance lines in Figure 1b. This excludes the possibility of dot A and B being located on the same channel edge.

We now present a tunnel spectroscopy of the electronic states in the two edge quantum dots. Figure 3a shows a color plot of $G_d(V_d, V_g)$ measured for $V_b = -2$ V. This plot is a stability diagram corresponding to the addition of the first four electrons to the edge quantum dots, that is, two electrons in dot A and two in dot B. The characteristic capacitances and the energy scales of both quantum dots can be extracted from such a plot. In particular, we measure charging energies $E_C^A = 26 \pm 1$ meV and $E_C^B = 17 \pm 1$ meV for dot A and B, respectively. These large values denote strong confinement potentials. Second we are able to extract the level arm parameters, expressing the channel potential difference when V_g is swept. They are found

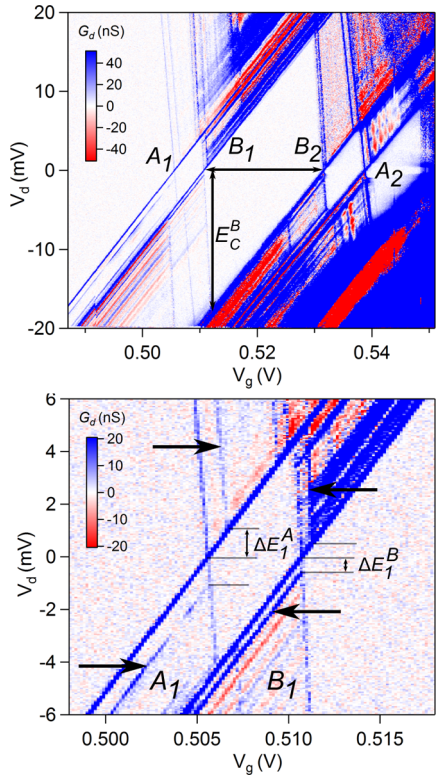

Figure 3. Top: Stability diagram for the first two electrons on the two edges at T = 0.1 K and $V_b = -2$ V. We extract the different capacitances and charging energies for both dots A and B. Bottom panel: Zoom showing the first excited states, depicted by the black arrows: ΔE_1^A (respectively ΔE_1^B) is the energy level spacing between the ground state A_1^g (respectively B_1^g) and the first excited state A_1^e (respectively B_1^e) of dot A (respectively B).

to be around 0.8 ± 0.1 for both dots. This value, close to maximum value of 1, also indicates the strong coupling of these dots to the front gate. The observed gate capacitance in the range of 8 aF corresponds roughly to a 24 nm long metallic edge state of radius 3 nm. We also estimate a mutual charging energy $E_C^m = 1.0 \pm 0.2$ meV, between dot A and dot B (see Supporting Information). Based on Figure 1b, the first electron goes into dot A (resonance A_1) and the second one in dot B (resonance B_1). Because dot B has a smaller charging energy, the filling order is reversed for the third and fourth electrons (resonances B_2 and A_2, respectively).

The stability diagram of Figure 3a gives access to the excitation energies of the quantum dots. In general, tunneling through an excited state results in a G_d resonance line parallel to a Coulomb edge. Many lines parallel to the diamond edges can be seen in Figure 3a, including negative G_d resonances (in red color). Most of these lines, however, do not correspond to excited states—which give positive differential conductance unless specific selection rules exist. They originate either from peaks (or dips) in the density of states of the heavily doped leads[8] or from environmental effects associated with nearby switching charges.[12] Figure 3b is a zoom-in of the region around the first Coulomb diamond, embedding conductance resonances A_1 and B_1. On the plot, G_d resonances depicted by the black arrows can be unambiguously attributed to tunneling via the first excited states of dot A and dot B, respectively. This identification relies on two properties of these lines: (i) they split in a magnetic field (see Figure 4b and discussion further

dx.doi.org/10.1021/nl500299h | Nano Lett. 2014, 14, 2094−2098

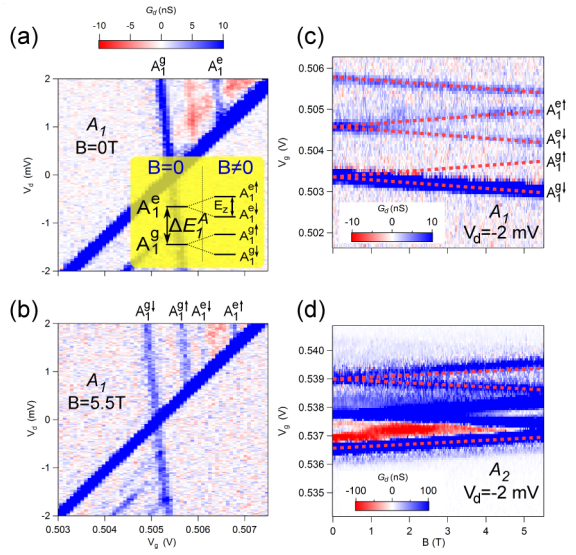

Figure 4. Magnetic field dependence for A_1 and A_2 resonances at T = 0.1 K. Left panel: The Coulomb diamonds are plotted for A_1 at B = 0 T (a) and 5.5 T (b). Both the ground and the first excited states are Zeeman split. The arrows indicate the Zeeman split levels at B = 5.5 T and the excited state at B = 0 T. Right panel: Differential conductance as function of B at V_d = −2 mV for A_1 (c) and A_2 (d). Dotted red lines represent the Zeeman shift for a spin ± (1/2)$\hbar$ expected for g-factor of 2. The shift of the low energy conductance line of the A_1 diamond means that the first electron is stabilized by the Zeeman effect. The Zeeman excited state is barely visible for A (line 2) due to the asymmetry in the tunnel rates to S−D ($\Gamma_S^A \leq \Gamma_D^A$). The first excited line is also Zeeman split. The upward shift of the low energy conductance line of the A_2 diamond means that the doubly occupied state is a singlet state (the second added electron as a spin (1/2)$\hbar$). This line is not split by the magnetic field. The high energy conductance line of the A_2 diamond is split by the magnetic field because the electron which exits the edge state can have both spin orientations. The inset in panel b shows schematically the energy diagram for the two lowest states of dot A.

below); (ii) the excited-state lines come in pairs, with the two lines of a pair (one line for $V_d > 0$ and the other line for $V_d < 0$) giving the same excitation energy. For dot A we measure an excitation energy ΔE_1^A = 1.0 ± 0.1 meV, which corresponds to the level spacing between the ground and the first excited orbital state. For dot B, the measured excitation energy is ΔE_1^B = 0.6 ± 0.1 meV.

Let us now discuss the nature of these excited states. These states might either be associated with spatial excitations in the confinement potential or with the valley−orbit splitting of the ground-state orbital. Indeed, the 6-fold conduction band valley degeneracy of bulk silicon is split by quantum confinement in the edge states. In these devices, the lowest-lying orbitals actually originate from the two Δ_x//[100] valleys perpendicular to the SOI substrate. In a simple effective mass picture, these two Δ_x valleys remain degenerate so that all states shall be at least 4-fold (spin + valley) degenerate.[13] The strong electric field at the edges can however lift the remaining valley degeneracy, an effect known as valley−orbit splitting.[14]

Since the effective mass approximation misses the valley−orbit splitting, we have performed an extra tight-binding calculation of the electronic structure of the nanowire in the potential extracted from the NEGF calculation at the bias corresponding to one electron in the channel. The tight-binding model of ref 15 is indeed able to capture the interactions between the different valleys of silicon. The confinement by the RC disorder results in spatial excitation energies averaging around 5 meV (depending on the configuration of disorder). The strong electric field of the gate (and, to a lower extent, remote charges) results in a valley-orbit splitting averaging around 0.8 meV. The measured excitation energies are, therefore, consistent with valley−orbit splitting but not with size quantization in the confinement potential. If they remain 1 order of magnitude smaller than those measured in single dopants,[16,17] this range of a few 100 μeV to 1 meV is consistent with recent results reported in very small intrinsic silicon structures.[18−20] The fact that no other excitations (e.g., to the next orbital level) are observed for dot A up to ∼4 meV supports this conclusion (the same consideration cannot be made for dot B due to the presence of a relatively dense set of lines most likely due to local density-of-state fluctuations in the leads).

The magnetic field dependence of the resonances gives an other, unambiguous proof of the low-energy excitations nature. Having associated ΔE_1 with the valley−orbit splitting, the only degeneracy left should come from the spin degree of freedom. Spin degeneracy can be lifted by a magnetic field due to the Zeeman effect. Figure 4a and b show a small region of the stability diagram around resonance A_1 for magnetic fields B = 0 and B = 5.5 T, respectively. The magnetic field induces a 2-fold Zeeman splitting of both the ground and the excited energy levels, which reveals their spin-1/2 character (see Figure 4b and the corresponding energy-level schematic in the inset). Within our experimental accuracy, the measured Zeeman splittings are identical and equal to the expected value for a Landé electron g-factor g = 2.

The full magnetic-field evolution of the spin-split resonances is shown in Figure 4c, where G_d is plotted as a function of (B,V_g) at V_d = −2 mV. The red dashed lines indicate the linear B-dependence expected from a Zeeman shift with g = 2, with positive and negative slopes corresponding to energy shifts $+g\mu_B B/2$ and $-g\mu_B B/2$, respectively. In particular, the bottom line, corresponding to the onset of tunneling from the source lead to the spin-down one-electron ground state of dot A, has a negative slope reflecting the field-induced energy lowering of the spin-down ground state level. The same negative slope is found in the top line, which corresponds to tunneling from the quantum dot ground state to the drain. In a similar measurement taken around the A_2 resonance, the slopes of the outer ground state resonances are positive as shown in Figure 4d. This behavior is perfectly consistent with a spin-singlet two-electron ground state corresponding to a double occupation of the first orbital level by two electrons with opposite spin.[21] In this case, the bottom line in Figure 4d corresponds to adding a spin-up electron to the spin-down one-electron ground state, while the top line corresponds to a spin-up electron tunneling out of the spin-singlet state and leaving the quantum dot in the spin-down one-electron ground state.

In summary, we have studied the formation and electronic properties of edge states in a trigate nanowire transistor. These edge states are studied in the single electron limit.[21−28] In the future the cross section can be made rounded or triangular to promote either a centered or single sharp edge channel. At low temperature, the one-dimensional edge modes localize into quantum dots due to the attractive confinement potential created by positive charge traps in the gate dielectric layers. These quantum dots exhibit large charging energies, and the spacing between the first two one-particle energy levels, of the

dx.doi.org/10.1021/nl500299h | Nano Lett. 2014, 14, 2094−2098

order of 1 meV, is ascribed to the valley−orbit splitting. These levels are consecutively filled by pairs of electrons, such that the quantum dot spin is 1/2 or 0 for odd or even occupancy, respectively. This filling is directly revealed by measurements in a finite magnetic field. Single charged edge quantum dots can thus open a promising route to spin qubits in intrinsic silicon.[29]

■ ASSOCIATED CONTENT

Supporting Information

Description of the fabrication process and measurement setup, role of surface roughness and remote Coulomb charges, and mutual charging energy between the two dots. This material is available free of charge via the Internet at http://pubs.acs.org.

■ AUTHOR INFORMATION

Corresponding Author

*E-mail: marc.sanquer@cea.fr. Phone: +33(0)4 38 78 43 67. Fax: +33(0)4 38 78 50 96.

Notes

The authors declare no competing financial interest.

■ ACKNOWLEDGMENTS

The authors acknowledge financial support from the EU through FP7MINECC initiative under Project TOLOP No 318397 and the ERC Starting Grant HybridNano and the French ANR under Project SIMPSSON No 2010-Blan-1015. The NEGF calculations were run at the TGCC/Curie machine using allocations from PRACE and GENCI.

■ REFERENCES

(1) Ferain, I.; Colinge, C. A.; Colinge, J.-P. *Nature* **2011**, *479*, 310−316.
(2) Xiong, W.; Park, J. W.; Colinge, J.-P. *IEEE Int. SOI Conf.* **2003**, 111−113.
(3) Fossum, J.; Yang, J.-W.; Trivedi, V. *IEEE Electron Device Lett.* **2003**, *24*, 745−747.
(4) Stadele, M.; Luyken, R. J.; Roosz, M.; Specht, M.; Rosner, W.; Dreeskornfeld, L.; Hartwich, J.; Hofmann, F.; Kretz, J.; Landgraf, E.; Risch, L. *Solid-State Dev. Res. Conf., ESSDERC* **2004**, 165−168.
(5) Roche, B.; Voisin, B.; Jehl, X.; Wacquez, R.; Sanquer, M.; Vinet, M.; Deshpande, V.; Previtali, B. *Appl. Phys. Lett.* **2012**, *100*, 032107−032109.
(6) Taur, Y. *IEEE Electron Device Lett.* **2000**, *21*, 245−247.
(7) Lansbergen, G. P.; Sellier, H.; Caro, J.; Collaert, N.; Ferain, I.; Jurczak, M.; Biesemans, S.; Rogge, S. *AIP Conf. Proc.* **2007**, *893*, 1397−1398.
(8) Pierre, M.; Wacquez, R.; Jehl, X.; Sanquer, M.; Vinet, M.; Cueto, O. *Nat. Nanotechnol.* **2010**, *5*, 133−137.
(9) Niquet, Y. M.; Nguyen, V. H.; Triozon, F.; Duchemin, I.; Nier, O.; Rideau, D. *J. Appl. Phys.* **2014**, *115*, 054512−054526.
(10) Casse, M.; Thevenod, L.; Guillaumot, B.; Tosti, L.; Martin, F.; Mitard, J.; Weber, O.; Andrieu, F.; Ernst, T.; Reimbold, G.; Billon, T.; Mouis, M.; Boulanger, F. *IEEE Trans. Electron Devices* **2006**, *53*, 759−768.
(11) Goodnick, S. M.; Ferry, D. K.; Wilmsen, C. W.; Liliental, Z.; Fathy, D.; Krivanek, O. L. *Phys. Rev. B* **1985**, *32*, 8171−8186.
(12) Pierre, M.; Hofheinz, M.; Jehl, X.; Sanquer, M.; Molas, G.; Vinet, M.; Deleonibus, S. *Eur. Phys. J. B* **2009**, *70*, 475−481.
(13) Ando, T.; Fowler, A. B.; Stern, F. *Rev. Mod. Phys.* **1982**, *54*, 437−672.
(14) Saraiva, A. L.; Calderon, M. J.; Capaz, R. B.; Hu, X.; Das Sarma, S.; Koiller, B. *Phys. Rev. B* **2011**, *84*, 155320−155329.
(15) Niquet, Y. M.; Rideau, D.; Tavernier, C.; Jaouen, H.; Blase, X. *Phys. Rev. B* **2009**, *79*, 245201−245212.
(16) Lansbergen, G. P.; Rahman, R.; Wellard, C. J.; Woo, I.; Caro, J.; Collaert, N.; Biesemans, S.; Klimeck, G.; Hollenberg, L. C. L.; Rogge, S. *Nat. Phys.* **2008**, *4*, 656−661.
(17) Roche, B.; Dupont-Ferrier, E.; Voisin, B.; Cobian, M.; Jehl, X.; Wacquez, R.; Vinet, M.; Niquet, Y.-M.; Sanquer, M. *Phys. Rev. Lett.* **2012**, *108*, 206812−206816.
(18) Xiao, M.; House, M. G.; Jiang, H. W. *Appl. Phys. Lett.* **2010**, *97*, 032103−032105.
(19) Yang, C. H.; Lim, W. H.; Lai, N. S.; Rossi, A.; Morello, A.; Dzurak, A. S. *Phys. Rev. B* **2012**, *86*, 115319−115323.
(20) Yang, C. H.; Rossi, A.; Ruskov, R.; Lai, N. S.; Mohiyaddin, F. A.; Lee, S.; Tahan, C.; Klimeck, G.; Morello, A.; Dzurak, A. S. *Nat. Commun.* **2013**, *4*, 2069.
(21) Lim, W. H.; Yang, C. H.; Zwanenburg, F. A.; Dzurak, A. S. *Nanotechnology* **2011**, *22*, 335704−335709.
(22) Ishikuro, H.; Hiramoto, T. *Appl. Phys. Lett.* **1997**, *71*, 3691−3693.
(23) Zhong, Z.; Fang, Y.; Lu, W.; Lieber, C. M. *Nano Lett.* **2005**, *5*, 1143−1146.
(24) Simmons, C. B.; Thalakulam, M.; Shaji, N.; Klein, L. J.; Qin, H.; Blick, R. H.; Savage, D. E.; Lagally, M. G.; Coppersmith, S. N.; Eriksson, M. A. *Appl. Phys. Lett.* **2007**, *91*, 213103−213105.
(25) Lim, W. H.; Zwanenburg, F. A.; Huebl, H.; Mottonen, M.; Chan, K. W.; Morello, A.; Dzurak, A. S. *Appl. Phys. Lett.* **2009**, *95*, 242102−242104.
(26) Zwanenburg, F. A.; van Rijmenam, C. E. W. M.; Fang, Y.; Lieber, C. M.; Kouwenhoven, L. P. *Nano Lett.* **2009**, *9*, 1071−1079.
(27) Borselli, M. G.; Eng, K.; Croke, E. T.; Maune, B. M.; Huang, B.; Ross, R. S.; Kiselev, A. A.; Deelman, P. W.; Alvarado-Rodriguez, I.; Schmitz, A. E.; Sokolich, M.; Holabird, K. S.; Hazard, T. M.; Gyure, M. F.; Hunter, A. T. *Appl. Phys. Lett.* **2011**, *99*, 063109−063111.
(28) Prati, E.; De Michielis, M.; Belli, M.; Cocco, S.; Fanciulli, M.; Kotekar-Patil, D.; Ruoff, M.; Kern, D. P.; Wharam, D. A.; Verduijn, J.; Tettamanzi, G. C.; Rogge, S.; Roche, B.; Wacquez, R.; Jehl, X.; Vinet, M.; Sanquer, M. *Nanotechnology* **2012**, *23*, 215204−215208.
(29) Zwanenburg, F. A.; Dzurak, A. S.; Morello, A.; Simmons, M. Y.; Hollenberg, L. C. L.; Klimeck, G.; Rogge, S.; Coppersmith, S. N.; Eriksson, M. A. *Rev. Mod. Phys.* **2013**, *85*, 961−1019.